

Direct observation of spin excitation anisotropy in the paramagnetic orthorhombic state of $\text{BaFe}_{2-x}\text{Ni}_x\text{As}_2$

Haoran Man,¹ Rui Zhang,¹ J. T. Park,² Xingye Lu,³ J. Kulda,⁴ A. Ivanov,⁴ and Pengcheng Dai^{1,3,*}

¹*Department of Physics and Astronomy, Rice University, Houston, Texas 77005, USA*

²*Heinz Maier-Leibnitz Zentrum, TU München, Lichtenbergstraße 1, D-85747 Garching, Germany*

³*Department of Physics, Center for Advanced Quantum Studies, Beijing Normal University, Beijing 100875, China*

⁴*Institut Laue-Langevin, 71 avenue des Martyrs, 38000 Grenoble, France*



(Received 31 December 2017; published 21 February 2018)

We use transport and inelastic neutron-scattering measurements to investigate single crystals of iron pnictide $\text{BaFe}_{2-x}\text{Ni}_x\text{As}_2$ ($x = 0, 0.03$), which exhibit a tetragonal-to-orthorhombic structural transition at T_s and stripe antiferromagnetic order at T_N ($T_s \geq T_N$). Using a tunable uniaxial pressure device, we detwin the crystals and study their transport and spin excitation properties at antiferromagnetic wave-vector $S_1(1,0)$ and its 90° rotated wave-vector $S_2(0,1)$ under different pressure conditions. We find that uniaxial pressure necessary to detwin and maintain the single domain orthorhombic antiferromagnetic phase of $\text{BaFe}_{2-x}\text{Ni}_x\text{As}_2$ induces resistivity and spin excitation anisotropy at temperatures above zero pressure T_s . In the uniaxial pressure-free detwinned sample, spin excitation anisotropy between $S_1(1,0)$ and $S_2(0,1)$ first appears in the paramagnetic orthorhombic phase below T_s . These results are consistent with predictions of spin nematic theory, suggesting the absence of structural or nematic phase transition above T_s in iron pnictides.

DOI: [10.1103/PhysRevB.97.060507](https://doi.org/10.1103/PhysRevB.97.060507)

In the phase diagrams of high-temperature superconductors, there are many exotic ordered phases which break spatial symmetries of the underlying lattice in addition to superconductivity [1]. One such phase is the electronic nematic phase which breaks orientational, but not translational, symmetry of the underlying lattice [2]. For iron pnictides, such as $\text{BaFe}_{2-x}\text{Ni}_x\text{As}_2$ [3,4], there exists a structural transition at T_s where the crystal structure changes from tetragonal to orthorhombic, followed by an antiferromagnetic (AF) transition at temperature T_N slightly below T_s ($T_N \leq T_s$) [5,6]. In the paramagnetic state above T_N , there is ample evidence for an electronic nematic phase from transport [7–12], magnetic torque [13], shear modulus [14], scanning tunneling microscopy [15,16], angle-resolved photoemission spectroscopy (ARPES) [17], nuclear magnetic resonance [18,19], and neutron-scattering experiments [20–24]. In particular, transport [7–12], ARPES [17], and neutron-scattering [20,22–24] experiments on single crystals of iron pnictides reveal that the nematic phase first appears below a characteristic temperature T^* above T_s and T_N where the system is in the paramagnetic tetragonal state. The nematic phase has been suggested as a distinct phase at T^* well above T_s [13]. Theoretically, it has been argued that the experimentally observed electronic nematic phase is due to spin [25–29] or orbital [30,31] degrees of freedom and should only appear in the paramagnetic orthorhombic phase below T_s .

To understand this behavior, we note that iron pnictides exhibiting tetragonal-to-orthorhombic structural transition form twin domains below T_s due to a small mismatch of the lattice constants of the orthorhombic axes (a and b) on the FeAs plane [16]. To unveil the intrinsic electronic properties of the

system, an external uniaxial pressure (stress) must be applied along the in-plane orthorhombic axis, forcing the short b axis to align with the external pressure, and drive the twinned domain sample into a single domain suitable for electronic anisotropy measurements [9]. Although an externally applied uniaxial pressure can effectively change the twin-domain population, it also introduces an artificial anisotropic strain field that breaks the fourfold rotational symmetry of the paramagnetic tetragonal phase and induces an orthorhombic lattice distortion in iron pnictides above T_s [23]. Although transport, neutron diffraction, and Raman scattering measurements carried out under tunable uniaxial pressure on single crystals of iron pnictides suggest that resistivity anisotropy found above T_s in transport measurements [7–12,14] is likely induced by the external pressure [32,33], much is still unclear concerning the nature of the nematic phase and its microscopic origin. In particular, if the electronic nematic phase has a spin origin, one would expect that spin excitation anisotropy at the AF ordering wave-vector $\mathbf{Q}_{\text{AF}} = S_1(1,0)$ and 90° rotated wave-vector $S_2(0,1)$ first appears below T_s with increasing spin-spin correlations at $S_1(1,0)$ and decreasing spin-spin correlations at $S_2(0,1)$ (Fig. 1) [27,28]. Although recent inelastic neutron-scattering experiments confirm the increasing spin-spin correlations at $S_1(1,0)$ and decreasing spin-spin correlations at $S_2(0,1)$ in electron-doped iron pnictide $\text{BaFe}_{1.935}\text{Ni}_{0.065}\text{As}_2$, the measurements were carried out under a uniaxial pressure and spin excitation anisotropy first appears at a temperature well above T_s [24]. Therefore, it is still unclear if spin excitation anisotropy above T_s is induced by the applied uniaxial pressure or an intrinsic property of the spin nematic phase in iron pnictides.

Our $\text{BaFe}_{2-x}\text{Ni}_x\text{As}_2$ ($x = 0, 0.03$) single crystals were grown using the self-flux method [Fig. 1(a)] [34]. The crystal

*pdai@rice.edu

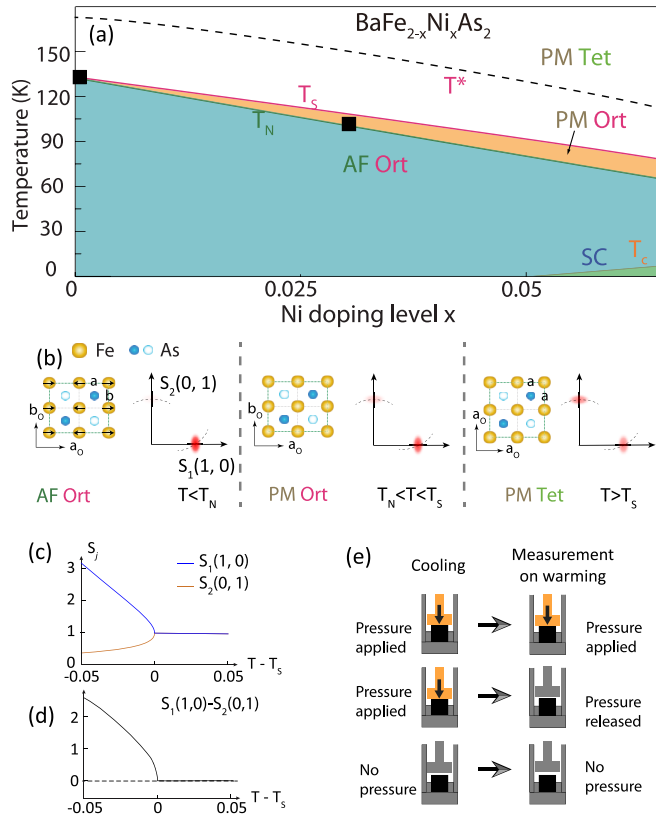


FIG. 1. (a) The electronic phase diagram of $\text{BaFe}_{2-x}\text{Ni}_x\text{As}_2$ as a function of Ni doping as determined from previous work [6]. The AF orthorhombic (AF Ort), paramagnetic orthorhombic (PM Ort), paramagnetic tetragonal (PM Tet), and superconductivity (SC) phases are clearly marked. The black square points mark the Ni-doping levels measured in this Rapid Communication. (b) Schematic of the Fe-As layer at different temperatures and its corresponding reciprocal space for temperatures $T < T_N$, $T_N > T > T_s$, and $T > T_s$. The AF ordering wave vector and its 90° rotation are marked as $S_1(1,0)$ and $S_2(0,1)$, respectively. The dotted curves are in-plane projection of neutron-scattering scan trajectories in reciprocal space. (c) Temperature dependence of the spin-spin correlation length at $S_1(1,0)$ (blue) and $S_2(0,1)$ (orange) across T_s as predicted by spin nematic theory [28]. (d) The corresponding temperature dependence of the magnetic intensity difference between $S_1(1,0)$ and $S_2(0,1)$. (e) Schematics of the *in situ* device used to change pressure on the sample. A micrometer and a spring are used to adjust the pressure applied to the sample [32]. The applied pressure can be released by a full retreat of the micrometer, leaving the sample partially detwinned at low temperatures.

orientations were determined by an x-ray Laue machine, and the square-shaped samples were cut for neutron-scattering and transport measurements. All samples were annealed at 800 K for 2 days to reduce defects and disorder. Transport measurements were carried out using a physical property measurement system. We used the standard four-probe method and measured resistivity on warming with a slow rate. The in-plane resistivity anisotropy was measured using the Montgomery method as described before [32]. By taking the first derivative of the resistivity data in $\text{BaFe}_{1.97}\text{Ni}_{0.03}\text{As}_2$ [Fig. 4(f)], we can see clear split of T_N and T_s with $T_N \approx 109$ and $T_s \approx 113$ K.

Using a specially designed tunable uniaxial pressure device [32], we study spin excitations at $S_1(1,0)$ and $S_2(0,1)$ and resistivity anisotropy in single domain orthorhombic $\text{BaFe}_{2-x}\text{Ni}_x\text{As}_2$ [Fig. 1(a)]. The nematic order parameter can be obtained by comparing the dynamic spin-spin correlation function $S(\mathbf{Q}, \omega)$ at $\mathbf{Q}_{\text{AF}} = S_1(1,0)$ and $\mathbf{Q}_2 = S_2(0,1)$ in the paramagnetic orthorhombic ($T_s > T > T_N$) and tetragonal ($T > T_s$) phases [Figs. 1(b)–1(d)] [28]. In the stress-free state, one expects that the differences in $S(\mathbf{Q}, \omega)$ at $S_1(1,0)$ and $S_2(0,1)$ would only occur below T_s [Figs. 1(c) and 1(d)] [28]. By measuring $S(\mathbf{Q}, \omega)$ at \mathbf{Q}_{AF} and $\mathbf{Q}_2 = S_2$ and comparing the outcome with transport measurements under different uniaxial pressures in $\text{BaFe}_{2-x}\text{Ni}_x\text{As}_2$, we find that applied uniaxial pressure indeed induces spin excitation anisotropy above T_s , and such anisotropy only appears below T_s in the pressure released sample, consistent with theoretical prediction [28]. Our transport and inelastic neutron-scattering experiments thus reveal a direct correlation between spin excitation and resistivity anisotropy, suggesting that resistivity anisotropy and the associated nematic phase have a spin origin [25–29].

We designed an *in situ* mechanical device which can apply and release uniaxial pressure at any temperature below 300 K [Fig. 1(e)] [32]. With a micrometer on top, the magnitude of the uniaxial pressure along the b axis of the orthorhombic lattice is controlled by a spring compressed by the displacement of the micrometer. By applying pressure at room temperature ($\gg T_s$), cooling the sample down below T_N , and releasing the pressure, we can measure the intrinsic electronic properties of iron pnictides in the AF ordered state without external pressure. Three types of measurements are carried out:

- (1) Pressure applied: Uniaxial pressure sufficient to detwin the sample is applied during the entire measurement. Both the intrinsic and the pressure-induced effect will contribute to measured transport and spin excitation anisotropy.
- (2) Pressure released: A uniaxial pressure is applied on cooling from room temperature to base temperature ($\ll T_N$). The pressure is then released at base temperature. Transport and spin excitation measurements were carried out on warming where the sample remains partially detwinned and only the intrinsic electronic difference in the orthorhombic state contributes to measured transport and spin excitation anisotropy.
- (3) No pressure: No uniaxial pressure is applied to the sample, and the sample remains in the twinned state below T_s and T_N . If twin domains are equally distributed, there should be no transport and spin excitation anisotropy.

Our inelastic neutron-scattering experiments were carried out at the IN8 triple-axis spectrometer using a multianalyzer detector system, Institut Laue-Langevin (ILL), Grenoble, France [35]. For inelastic neutron-scattering experiments, annealed square-shaped single crystals of BaFe_2As_2 (~ 220 mg) or $\text{BaFe}_{1.97}\text{Ni}_{0.03}\text{As}_2$ (~ 200 mg) were mounted on the sample stick specially designed for applying uniaxial pressure (along the b axis) inside an orange cryostat [32]. The momentum transfer \mathbf{Q} in three-dimensional reciprocal space in \AA^{-1} is defined as $\mathbf{Q} = H\mathbf{a}^* + K\mathbf{b}^* + L\mathbf{c}^*$, where H , K , and L are Miller indices and $\mathbf{a}^* = \hat{\mathbf{a}}2\pi/a$, $\mathbf{b}^* = \hat{\mathbf{b}}2\pi/b$, $\mathbf{c}^* = \hat{\mathbf{c}}2\pi/c$ with $a \approx b \approx 5.549$ and $c \approx 12.622$ \AA [6]. In the AF ordered state of a fully detwinned sample, the AF Bragg peaks occur at $(\pm 1, 0, L)$ ($L = 1, 3, 5, \dots$) positions in reciprocal space and are absent at $(0, \pm 1, L)$. The sample was aligned on the

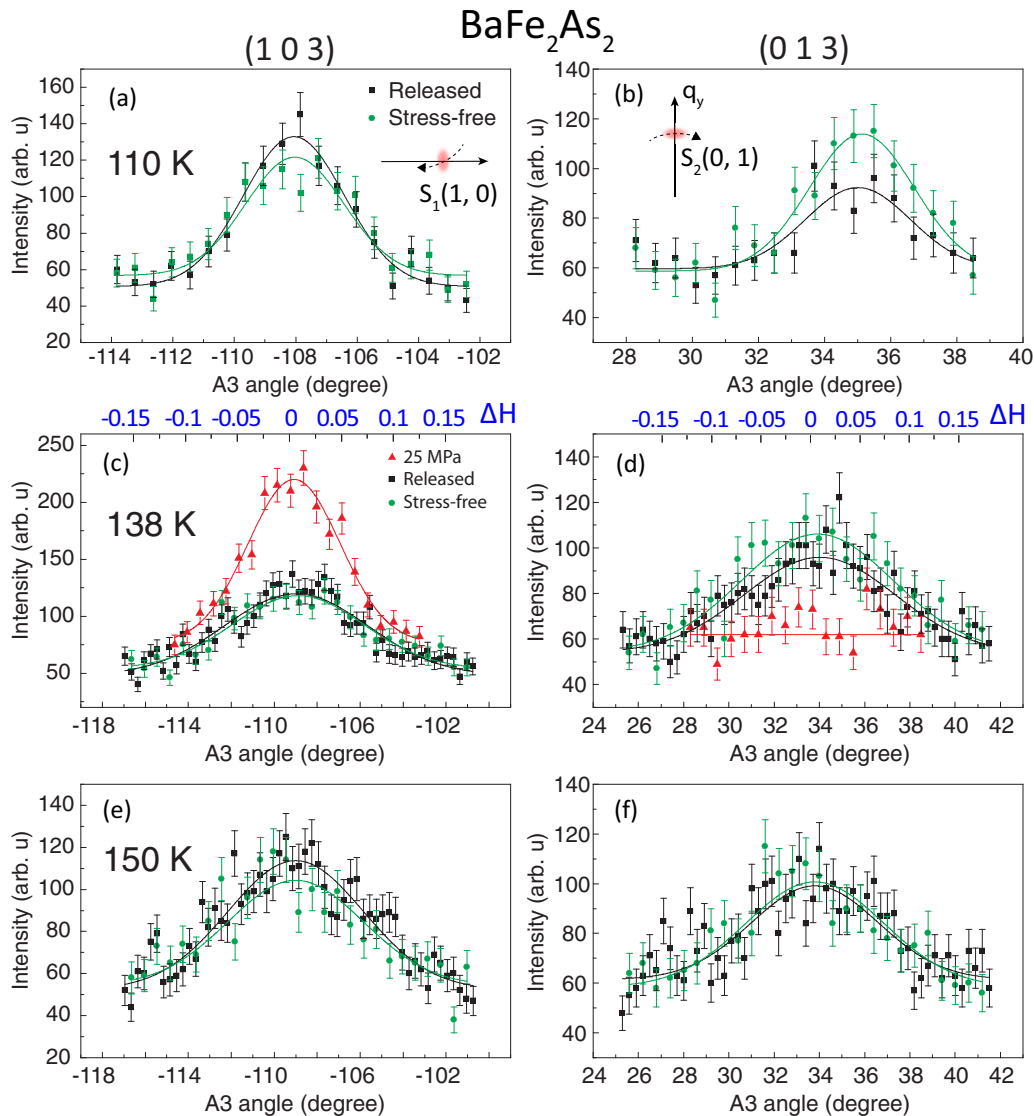


FIG. 2. Inelastic neutron-scattering measurements of 10-meV spin excitations of BaFe_2As_2 under different conditions at $S_1(1,0)$ and $S_2(0,1)$. Transverse A_3 (rocking) scans at different temperature and pressure conditions. The corresponding wave-vector directions in reciprocal space are shown in the insets of (a) and (b). The scans are measured under 25 MPa pressure (red), pressure-released (black), and stress-free (green) cases. (a) and (b) at 110 K ($<T_N/T_S$), (c) and (d) 138 K ($\approx T_N/T_S$), and (e) and (f) 150 K ($>T_N/T_S$).

$[H,0,L]$ scattering plane. With the goniometer below the orange cryostat and with extra coverage provided by the flat-cone setup on IN8 [35], we can access both (1,0,3) and (0,1,3) around 10 meV and (1,0,5), (0,1,5) magnetic Bragg peak positions at 0 meV.

We have collected neutron-scattering data under three different conditions: (1) under 22–25 MPa uniaxial pressure (pressured), (2) pressure released at 10 K and no pressure measurements on warming (released), and (3) no pressure at all temperatures (stress free) [Fig. 1(e)]. For each scenario, spin excitations at wave-vectors (1,0,3) and (0,1,3) are measured in the same warm-up cycle. We first test if spin excitation anisotropy seen above T_N/T_S in uniaxial pressured BaFe_2As_2 [20] also exists in the pressure-released situation. Figures 2(a) and 2(b) compare transverse scans of spin excitations at 10 meV and 110 K ($<T_N$) for the pressure-released

and stress-free cases at wave-vectors $S_1(1,0)$ and $S_2(0,1)$, respectively. Assuming spin excitations are isotropic in the stress-free situation, we find clear spin excitation anisotropy in the pressure-released situation, consistent with previous elastic-scattering measurements below T_N [32]. On warming to 138 K at T_N/T_S , spin excitations in the pressured case double that of the stress-free case and only exist at $S_1(1,0)$, consistent with a fully pressure-induced detwinned state [Figs. 2(c) and 2(d)] [20]. For comparison, transverse scans in the pressure-released and stress-free cases are indistinguishable. Upon further warming up to 150 K above T_N/T_S , we again find no spin excitation anisotropy at $S_1(1,0)$ and $S_2(0,1)$ [Figs. 2(e) and 2(f)], suggesting that spin excitation anisotropy only appears below T_N/T_S in the pressure-released case.

To confirm these results, we carried out spin excitation measurements in these three pressure conditions using long

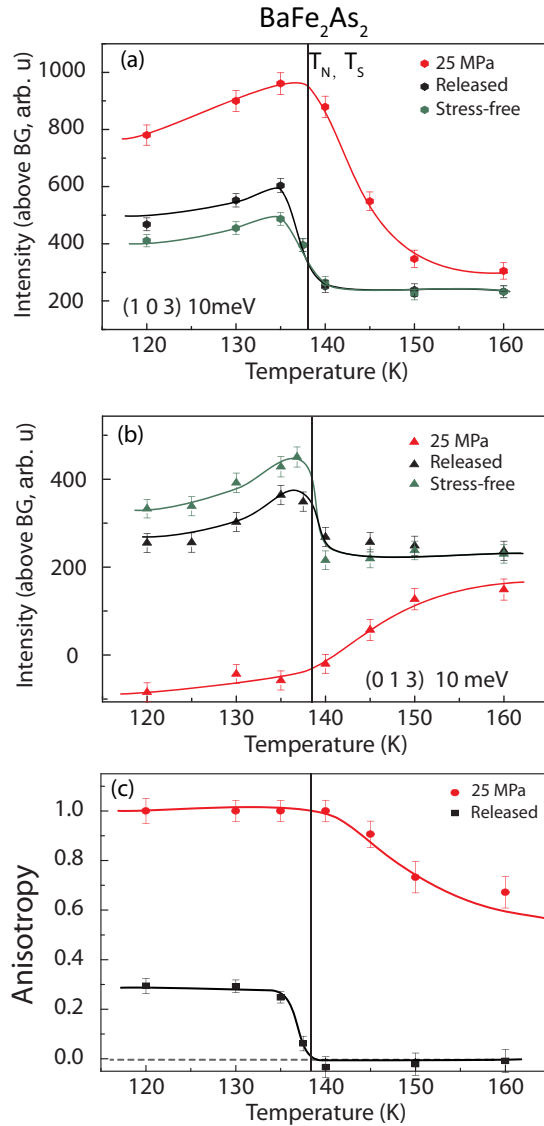


FIG. 3. Temperature dependence of spin excitations at 10 meV in BaFe₂As₂ under 25 MPa uniaxial pressure, pressure-released, and stress-free conditions at (a) AF wave-vector S₁(1,0) = (1,0,3) and (b) S₂(0,1) = (0,1,3). The negative scattering is due to imperfect background scattering subtraction. (c) Temperature dependence of spin excitation anisotropy under 25 MPa pressure and pressure released.

counting times at the peak center and subtracted background points. Figures 3(a) and 3(b) show the background subtracted peak intensities at S₁(1,0) = (1,0,3) and S₂(0,1) = (0,1,3), respectively. In case one under 25 MPa uniaxial pressure (red), the large spin excitation anisotropy at S₁(1,0) and S₂(0,1) below T_N/T_s persists to temperatures well above T_N/T_s, consistent with earlier results [20]. For case two pressure-released measurements (black), although the spin excitation anisotropy between S₁(1,0) = (1,0,3) and S₂(0,1) = (0,1,3) becomes much smaller compared with the stress-free case, it is still present below 138 K but vanishes above 138 K at both wave vectors. By normalizing pressured and released data with stress-free measurements at S₁(1,0) and S₂(0,1), we can estimate the spin excitation anisotropy η using $\eta =$

$(I_{(1,0)} - I_{(0,1)}) / (I_{(1,0)} + I_{(0,1)})$, where I_(1,0) and I_(0,1) are spin excitations at S₁(1,0) and S₂(0,1), respectively. For a fully detwinned sample in the stress-free AF ordered state, only I_(1,0) should be present and $\eta = 1$. In the stress-free paramagnetic tetragonal state, we expect I_(1,0) = I_(0,1) and $\eta = 0$. Figure 3(c) indicates that uniaxial pressure is necessary to maintain a 100% detwinned state in BaFe₂As₂. Although spin excitations still have anisotropy in the pressure-released case below T_N/T_s, the anisotropy completely vanishes above T_N/T_s. These measurements confirm that spin excitation anisotropies above T_N/T_s are entirely induced by externally applied uniaxial pressure.

Having established the vanishing spin excitation anisotropy in the paramagnetic state of BaFe₂As₂, where T_N ≈ T_s without applied uniaxial pressure, it is interesting to ask if spin excitations can be anisotropic in the external pressure free paramagnetic orthorhombic nematic phase as predicted by spin nematic theory [25–29]. For this experiment, we chose BaFe_{1.97}Ni_{0.03}As₂ because of its separated T_N and T_s (>T_N) [Fig. 4(f)] [6]. Figures 4(a) and 4(b) show temperature dependence of the magnetic scattering at 10 meV for S₁(1,0) = (1,0,3) and S₂(0,1) = (0,1,3), respectively. Similar to the measurement on BaFe₂As₂, spin excitation anisotropy under 22 MPa uniaxial pressure (red) extends to temperatures well above T_s [Figs. 4(a), 4(b) and 4(d)]. However, the pressure-released data (black) are much closer to the stress-free data on approaching T_s. For temperatures above T_s, there are no detectable differences between S₁(1,0) and S₂(0,1) as seen in Fig. 4(d). Therefore, spin excitations exhibit a weak anisotropy in the paramagnetic orthorhombic phase of BaFe_{1.97}Ni_{0.03}As₂, consistent with theoretical expectation for a spin excitation driven nematic phase [25–29]. For comparison, Fig. 4(c) shows temperature dependence of the resistivity anisotropy obtained under 22 MPa uniaxial pressure (red) and pressure-released (black) conditions. For the pressure-released case, we find no evidence of time-dependent relaxation of the resistivity anisotropy within several hours. Although resistivity anisotropy reduces dramatically in the pressure-released case, it is still present in a narrow temperature region above T_s and below ~130 K due possibly to the residual anisotropic strain in the pressure-released sample [Fig. 4(c)] [32]. Since increasing uniaxial pressure enhances both the resistivity and the spin excitation anisotropy, there must be a direct correlation between the resistivity and the spin excitation anisotropy.

To further test if the spin-spin correlation length also increases at S₁(1,0) but decreases at S₂(0,1) below T_s as expected from the spin nematic theory [27–29] [Fig. 1(c)] [27,28], we show in Fig. 4(e) temperature dependence of the full width at half maximum (FWHM) of spin excitations at 10 meV along the marked scan directions at S₁(1,0) and S₂(0,1). At both wave vectors, we find a clear reduction of the FWHM in spin excitations around T_s. However, since the data collected at S₂(0,1) are along the transverse direction, we cannot directly compare the outcome with spin nematic theory, which predicted an increase in the spin-spin excitation correlation length measurable for scans along the longitudinal direction.

To summarize, by using a specially designed *in situ* detwining device to tune the applied uniaxial pressure, we study spin excitation and resistivity anisotropy in AF order and paramagnetic phases of BaFe_{2-x}Ni_xAs₂. For the

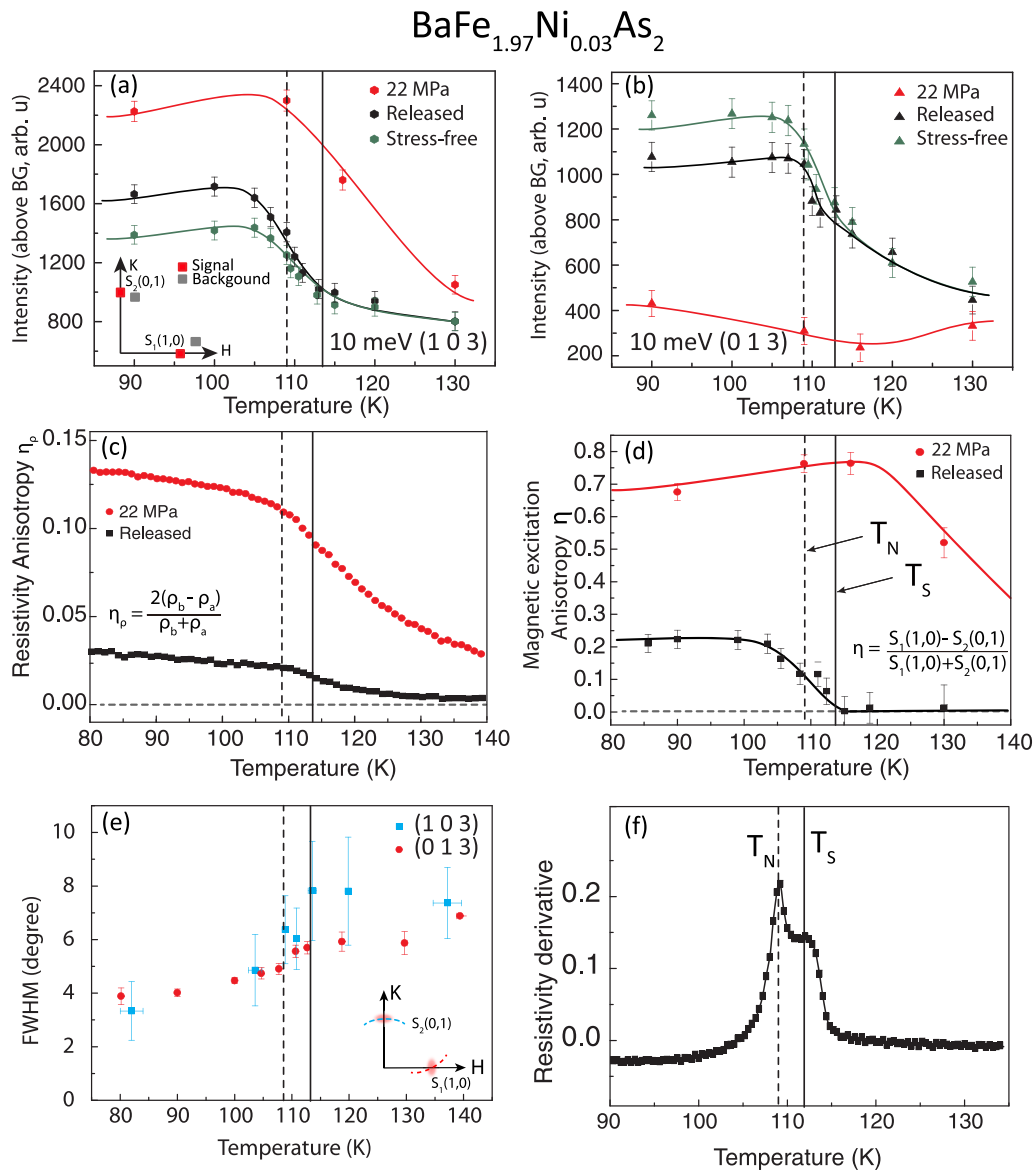


FIG. 4. Temperature dependence of resistivity and spin excitation anisotropy for $\text{BaFe}_{1.97}\text{Ni}_{0.03}\text{As}_2$. (a) Temperature dependence of the 10-meV spin excitations under 22 MPa, released, and stress-free conditions at $S_1(1,0)$. (b) Similar measurements at $S_2(0,1)$. Temperature dependence of the (c) resistivity and (d) spin excitation anisotropy under 22 MPa and pressure-released conditions. (e) Temperature dependence of the FWHM of the 10-meV spin excitations at $S_1(1,0)$ and $S_2(0,1)$. The scan directions are marked by the dotted curve in the inset. (f) Temperature dependence of the first derivative of resistivity, where T_N and T_S are marked as vertical lines.

undoped parent compound BaFe_2As_2 with $T_N \approx T_S$, we find clear spin excitation anisotropy in the pressure-released AF ordered phase at 10 meV, but anisotropy vanishes in the paramagnetic tetragonal phase. For pressure-released electron-doped $\text{BaFe}_{1.97}\text{Ni}_{0.03}\text{As}_2$ with $T_N < T_S$, the spin excitation anisotropy at 10 meV present in the AF ordered phase decreases on warming, persists in the paramagnetic orthorhombic phase ($>T_N$) before vanishing in the paramagnetic tetragonal state above T_S . Assuming the small resistivity anisotropy above T_S in the pressure-released sample is an extrinsic effect due to residual strain, our results establish a direct correlation between spin excitation and resistivity anisotropy and are consistent with predictions of spin nematic theory [25–29].

Therefore, our data indicate no additional phase transition above T_S , and suggest that the observed resistivity anisotropy in the paramagnetic tetragonal phase [7–12] arises from strong magnetoelastic coupling due to the presence of strong nematic fluctuations.

We are grateful to S. Turc, E. Bourgeat-Lami, and E. Lelièvre-Berna of ILL, France for designing and constructing the detwinning device used at IN8. The neutron-scattering work at Rice University was supported by the US NSF Grant No. DMR-1700081 (P.D.). The $\text{BaFe}_{2-x}\text{Ni}_x\text{As}_2$ single-crystal synthesis work at Rice University was supported by the Robert A. Welch Foundation Grant No. C-1839 (P.D.).

- [1] B. Keimer, S. A. Kivelson, M. R. Norman, S. Uchida, and J. Zaanen, *Nature (London)* **518**, 179 (2015).
- [2] E. Fradkin, S. A. Kivelson, M. J. Lawler, J. P. Eisenstein, and A. P. Mackenzie, *Annu. Rev. Condens. Matter Phys.* **1**, 153 (2010).
- [3] G. R. Stewart, *Rev. Mod. Phys.* **83**, 1589 (2011).
- [4] P. C. Dai, *Rev. Mod. Phys.* **87**, 855 (2015).
- [5] H. Luo, R. Zhang, M. Laver, Z. Yamani, M. Wang, X. Lu, M. Wang, Y. Chen, S. Li, S. Chang, J. W. Lynn, and P. C. Dai, *Phys. Rev. Lett.* **108**, 247002 (2012).
- [6] X. Lu, H. Gretarsson, R. Zhang, X. Liu, H. Luo, W. Tian, M. Laver, Z. Yamani, Y.-J. Kim, A. H. Nevidomskyy, Q. Si, and P. C. Dai, *Phys. Rev. Lett.* **110**, 257001 (2013).
- [7] J. H. Chu *et al.*, *Science* **329**, 824 (2010).
- [8] M. A. Tanatar, E. C. Blomberg, A. Kreyssig, M. G. Kim, N. Ni, A. Thaler, S. L. Bud'ko, P. C. Canfield, A. I. Goldman, I. I. Mazin, and R. Prozorov, *Phys. Rev. B* **81**, 184508 (2010).
- [9] I. R. Fisher, L. Degiorgi, and Z. X. Shen, *Rep. Prog. Phys.* **74**, 124506 (2011).
- [10] J. H. Chu, H.-H. Kuo, J. G. Analytis, and I. R. Fisher, *Science* **337**, 710 (2012).
- [11] H.-H. Kuo, M. C. Shapiro, S. C. Riggs, and I. R. Fisher, *Phys. Rev. B* **88**, 085113 (2013).
- [12] H.-H. Kuo, J.-H. Chu, S. A. Kivelson, and I. R. Fisher, *Science* **352**, 958 (2016).
- [13] S. Kasahara, H. J. Shi, K. Hashimoto, S. Tonegawa, Y. Mizukami, T. Shibauchi, K. Sugimoto, T. Fukuda, T. Terashima, A. H. Nevidomskyy, and Y. Matsuda, *Nature (London)* **486**, 382 (2012).
- [14] A. E. Böhmer and C. Meingast, *C. R. Phys.* **17**, 90 (2016).
- [15] E. P. Rosenthal, E. F. Andrade, C. J. Arguello, R. M. Fernandes, L. Y. Xing, X. C. Wang, C. Q. Jin, A. J. Millis, and A. N. Pasupathy, *Nat. Phys.* **10**, 225 (2014).
- [16] C. Cantoni, M. A. McGurie, B. Sparov, A. F. May, T. Keiber, F. Bridges, A. S. Sefat, and B. C. Sales, *Adv. Mater.* **27**, 2715 (2015).
- [17] M. Yi, Y. Zhang, Z.-X. Shen, and D. H. Lu, *npj Quantum Materials* **2**, 57 (2017).
- [18] M. Fu, D. A. Torchetti, T. Imai, F. L. Ning, J.-Q. Yan, and A. S. Sefat, *Phys. Rev. Lett.* **109**, 247001 (2012).
- [19] A. P. Dioguardi, T. Kissikov, C. H. Lin, K. R. Shirer, M. M. Lawson, H.-J. Grafe, J.-H. Chu, I. R. Fisher, R. M. Fernandes, and N. J. Curro, *Phys. Rev. Lett.* **116**, 107202 (2016).
- [20] X. Y. Lu, J. T. Park, R. Zhang, H. Q. Luo, A. H. Nevidomskyy, Q. Si, and P. C. Dai, *Science* **345**, 657 (2014).
- [21] Q. Zhang, R. M. Fernandes, J. Lamsal, J. Yan, S. Chi, G. S. Tucker, D. K. Pratt, J. W. Lynn, R. W. McCallum, P. C. Canfield, T. A. Lograsso, A. I. Goldman, D. Vaknin, and R. J. McQueeney, *Phys. Rev. Lett.* **114**, 057001 (2015).
- [22] Y. Song, X. Lu, D. L. Abernathy, D. W. Tam, J. L. Niedziela, W. Tian, H. Luo, Q. Si, and P. Dai, *Phys. Rev. B* **92**, 180504(R) (2015).
- [23] X. Lu, K.-F. Tseng, T. Keller, W. Zhang, D. Hu, Y. Song, H. Man, J. T. Park, H. Luo, S. Li, A. H. Nevidomskyy, and P. Dai, *Phys. Rev. B* **93**, 134519 (2016).
- [24] W. L. Zhang, J. T. Park, X. Y. Lu, Y. Wei, X. Ma, L. Hao, P. C. Dai, Z. Meng, Y. F. Yang, H. Luo, and S. Li, *Phys. Rev. Lett.* **117**, 227003 (2016).
- [25] C. Fang, H. Yao, W.-F. Tsai, J. P. Hu, and S. A. Kivelson, *Phys. Rev. B* **77**, 224509 (2008).
- [26] C. Xu, M. Muller, and S. Sachdev, *Phys. Rev. B* **78**, 020501 (2008).
- [27] R. M. Fernandes, A. V. Chubukov, and J. Schmalian, *Nat. Phys.* **10**, 97 (2014).
- [28] R. M. Fernandes and J. Schmalian, *Supercond. Sci. Technol.* **25**, 084005 (2012).
- [29] S. Liang, A. Moreo, and E. Dagotto, *Phys. Rev. Lett.* **111**, 047004 (2013).
- [30] C.-C. Lee, W.-G. Yin, and W. Ku, *Phys. Rev. Lett.* **103**, 267001 (2009).
- [31] W. Lv, J. Wu, and P. Phillips, *Phys. Rev. B* **80**, 224506 (2009).
- [32] H. Man, X. Lu, J. S. Chen, R. Zhang, W. Zhang, H. Luo, J. Kulda, A. Ivanov, T. Keller, E. Morosan, Q. Si, and P. Dai, *Phys. Rev. B* **92**, 134521 (2015).
- [33] X. Ren, L. Duan, Y. Hu, J. Li, R. Zhang, H. Luo, P. Dai, and Y. Li, *Phys. Rev. Lett.* **115**, 197002 (2015).
- [34] Y. C. Chen, X. Y. Lu, M. Wang, H. Q. Luo, and S. L. Li, *Supercond. Sci. Technol.* **24**, 065004 (2011).
- [35] M. Boehm, P. Steffens, J. Kulda, M. Klicpera, S. Roux, P. Courtois, P. Svoboda, J. Saroun, and V. Sechovsky, *Neutron News* **26**, 18 (2005).